Hydrodynamic Modeling of LMRS Unmanned Underwater Vehicle and Tow Tank Test Validation

Yuh-Lin Hwang

The Boeing Company
3370 Miraloma Avenue
Anaheim, CA 92803, U.S.A.
yuh-lin.hwang@boeing.com

***Abstract*-A rapid engineering method using body build-up approach to predict nonlinear hydrodynamic forces and moments on the Long Term Mine Reconnaissance System (LMRS) autonomous, unmanned underwater vehicle (UUV) is presented. Semi-empirical equations representing the hydrodynamic model for calculating loads on UUV's geometric components, such as bare body, control fins, recovery ring, and Thrust-Vectored Pumpjet (TVPJ) propulsor are described. Numerical results of the predicted total forces and moments on the vehicle are presented over a range of angle of attacks, vehicle speeds, control fin deflections, and propulsion ratios. The hydrodynamic performances of the vehicle were studied. The results indicated that the vehicle stability tends to decrease with increasing speed, and the control fin effectiveness decreases with decreasing speed and propulsion ratio. Excellent agreement was obtained between the predicted results and test data measured from full-scale model testing conduced at David Taylor Model Basin. The results of the study and tow tank test are described.**

I. INTRODUCTION

The LMRS UUV operates clandestinely from a submarine and is capable of being launched and recovered through submarine's torpedo tube for mine surveillance and data reconnaissance. The design of the UUV to achieve safe separation launch, reliable recovery, and meet a high level of maneuvering performance in its mission execution activities relies on the knowledge and successful prediction of the configuration hydrodynamic characteristics of the vehicle. A rapid engineering method using body build-up approach for the LMRS UUV configuration has been developed to predict both linear and nonlinear hydrodynamic coefficients for the analyses of vehicle motion performance, stability, and control system. This method is based on theoretical formulations supplemented through reference to experimental data and/or computational fluid dynamics (CFD).

The body build-up technique [1,2,3] predicts the overall hydrodynamic loads on the vehicle, considering individual contributions from UUV's geometric components and interference effects between components. Existing semi-empirical equations were utilized to calculate the loads on the isolated components, such as vehicle body, fins, and recovery ring, while the hydrodynamic model of TVPJ was derived based on the momentum theory to predict the TVPJ effects on the vehicle hydrodynamic characteristics.

II. LMRS UUV GEOMETRY

The baseline design of the LMRS UUV consists of a torpedo shaped body, four inner control fins, four outer control fins, a recovery ring with four support struts, and a TVPJ propulsor. The assembly of TVPJ consists of shroud, rotor and stators. The control fins are arranged in X-tail configuration and the ring support struts are arranged in cruciform configuration. The overview of the vehicle is shown in Fig. 1. The overall length of the vehicle is 6.1 meters (240 inches) and the maximum diameter is 0.532 meters (20.95 inches) with a displacement of approximately 1250 kilograms (2750 lbs).

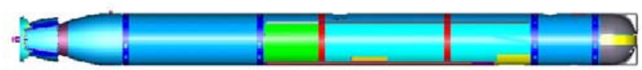

Fig. 1 Baseline LMRS UUV

III. HYDRODYNAMIC REPRESENTATIONS

A. Isolated Vehicle Body Model

The hydrodynamic loads on the a body of revolution at angle of attack α are usually described in terms of a normal force, a pitch and an axial force. Past studies [4,5,6] have been quite successfully to show that the normal force can be described adequately by a linear potential flow term and a nonlinear crossflow drag term. At small angles of attack less than approximately 4^o, the normal force is well approximated by potential flow theory and is linear with angle of attack. When angle reaches approximately 4^o, the crossflow begins to separate initially near the base of the body, and eventually the separation region extends over the entire body as angle of attack increases. For LMRS UUV at speed of U and angle of attack of α, the total normal force, NF, on the isolated body can be expressed as [1,2]

$$NF = \frac{\rho}{2} U^2 [2(k_2 - k_1) S_b \alpha + Cdc_{ave} S_{pc} \sin^2 \alpha] \qquad (1)$$

In the linear term, $(k_2 - k_1)$ is the apparent mass factor of Munk [4] and S_b is the cross-sectional area of equivalent base caused by boundary layer thickening or separation. The location of the thickening may be determined by the use of a computational fluid dynamics (CFD) code or from the semi-empirical equation given in SEAHAC TR 79-1 [7] or test data in [2]. In the nonlinear term, S_{pc} is the planform area of that portion of the body in separated crossflow, and Cdc is the average crossflow drag coefficient over the entire separated region. The computed non-dimensional normal forces versus angle of attack for the LMRS UUV body at speed of 6 knots are presented in Fig. 2.

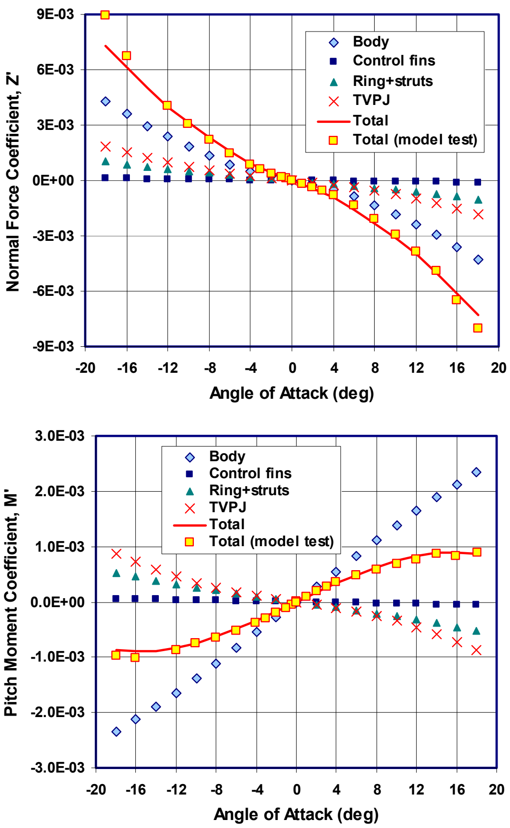

Fig. 2 Predicted normal force and pitch moment at speed of 6 knots

The pitch moment on the body is obtained by integrating the axial distribution of the normal force along the vehicle length, L. The total pitch moment about a reference point $Xref$ can be described by a potential flow term and a viscous flow term in the following form [2]

$$Moment = \frac{\rho}{2}U^2 [2k_m(k_2 - k_1)\alpha \int_0^{X_{sa}} \frac{dS}{dx}(x_{ref} - x)dx + 4\sin^2\alpha (\frac{L}{L - X_{sc}}) \int_{Xsc}^{L} Cdc\ (x_{ref} - x)R(x)dx] \quad (2)$$

where S is the local cross-sectional area of body and R is the local body radius, k_m is an empirical factor for LMRS UUV applied to apparent mass term. X_{sa} and X_{sc} are the axial locations of axial flow and crossflow separations, respectively. Figure (2) shows the computed pitch moments for the LMRS UUV body at 6-knot speed.

From (1) and (2), the non-dimensional static coefficients, such as Z'w and M'w for the isolated body can be determined. The rotary coefficients, Z'q and M'q, may be determined from the Strumpf formulae given in [8]

$$Z'_q = k' Z'_w (x_{sa} - x_{ref}) / L;$$
$$M'_q = k' Z'_w [(x_{sa} - x_{ref}) / L]^2 \quad (3)$$

The axial force has relatively little variation with angle of attack up to at least 15° [2] compared to the normal force and pitch moment. It can be described adequately by a skin friction term and a form drag term. Granville method in SEAHAC [7] was used for the calculation of the vehicle drag.

B. *Fin Lift Model*

Each LMRS control fin is split into an inner part and an outer part, as shown in Fig. 3. The inner fin is a flapped control surface and inside the shroud in the propeller slipstream. The outer fin is all-movable and outside the shroud in the free stream. The fin lift varies as a function of angle of attack, α, effective aspect ratio, AR, flow velocity over the fin, U_f, sweep angle, flap deflection, δ, tip shape, taper ratio, and fin-boy mutual interactions. The fin lift coefficient, C_L, can be described adequately [9,10] by a linear term and a cross flow term as

$$C_L = [(\frac{\partial C_L}{\partial \alpha})_{\alpha=0}\alpha + \frac{C_{Dc}}{AR}\sin^2\alpha](K_{wb} + K_{bw})(\frac{Uf}{U})^2 \frac{\partial \alpha}{\partial \delta} \quad (4)$$

where C_{Dc} is crossflow drag coefficients dependent on tip shape and taper ratio [10]. The body carryover factor for fin, K_{bw}, and the fin interference factor for body, K_{wb} may be estimated from Pitts-Nielsen-Kaattari (PNK) method [3,11,12]. The computed forces and moments on the vehicle induced by control fins at various angles of attack are shown in Fig. 2 for speed of 6 knots

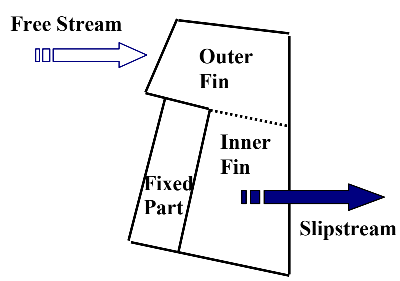

Fig. 3 Control Fin

C. *Recovery Ring Model*

The recovery ring has a significant effect on the dynamics and stability of the vehicle. The lift coefficient for the ring as currently design can be estimated by the method of McCormick's [13] for a ring-wing body combination as shown in Fig. 4. The ring lift varies as a function of angle of attack, α, ring radius, R_2, body radius, R_1, chord, C, and slope of section lift coefficient, a. The forces and moments induced by the recovery ring and its support struts for speed of 6 knots are shown in Fig. 2.

$$C_L = \frac{L}{qS} = \frac{2a(1-r^2)}{1+\frac{a}{\pi AR}(1-r^2)}\alpha \quad (5)$$

$$S = \frac{\pi R_2 C}{2};\ AR = \frac{8R_2}{\pi C};\ r = \frac{R_1}{R_2};\ q = \frac{1}{2}\rho U^2$$

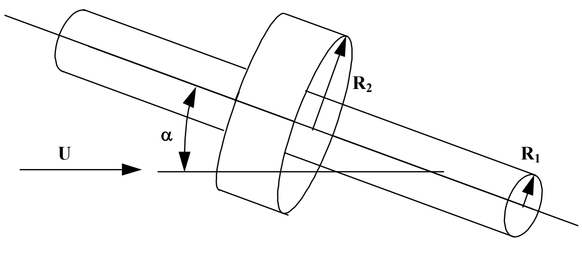

Fig. 4 Ring-Wing-Body Model

D. TVPJ Propulsor Model

When a propulsor is appended to a vehicle, it changes vehicle's motion characteristics. The TVPJ propulsor on the LMRS vehicle generates thrust as well as lift, drag and moment. The lift force can be large and it has an important effect on the stability of the vehicle. To predict the TVPJ effects on the hydrodynamics of the vehicle, a semi-empirical method using momentum theory was developed to compute the propulsor lift and moments on the vehicle at both the self-propulsion and off-propulsion points.

The level of the lift and thrust is dependent upon the angle of attack of the TVPJ system. The TVPJ generates thrust by imparting the velocity to the mass of fluid passing through the propeller disk. If the fluid is deflected downward as shown in Fig. 5, then a lift force is produced. The levels of the lift produced will depend on the mass of fluid passing through the propeller disk and velocity imparted in the propeller slipstream, U_2.

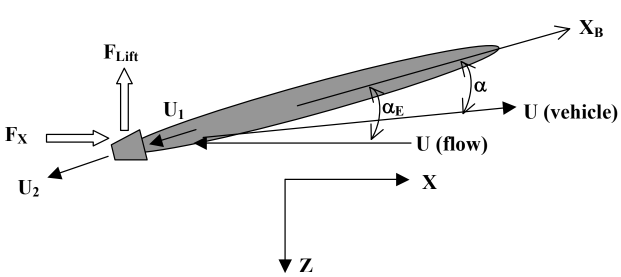

Fig. 5 Lift force of TVPJ propulsor

Figure 5 depicts a vehicle at an angle of attack of α with velocity of U. The mass flow rate, M_E, passing through the propulsor depends upon the angle of the flow on the body, α_E, at the inlet of TVPJ and can be expressed in the following manner:

$$M_E = Cm\ Q\ exp(|\alpha_E|) \quad (6)$$

$$Cm = mass\ flow\ rate / Q \quad (7)$$

$$Q = \rho U A \quad (8)$$

where Cm is the non-dimensional mass flow rate at zero angle of attack, A is the maximum cross sectional area of vehicle, and ρ is the density of fluid. The inlet flow angle on the vehicle body, α_E , derived to correlate the model test data for the LMRS UUV is given by

$$\alpha_E = \alpha \exp(|\alpha (U/6)^{1.5}|), \quad \text{for } \alpha < 20° \quad (9)$$

or $\alpha_E = 2\alpha$, if $\exp(|\alpha (U/6)^{1.5}|) > 2$ (10)

It is assumed that the TVPJ propulsor will generate a constant thrust, T, for a specific RPM at any pitching attitude, and not stall below the angle of attack of 20 degrees. The drag and moments of the TVPJ itself are neglected in the presented study. Then the lift force F_{Lift}, axial force F_X in the X direction, and the average speed of slipstream U_2 can be derived for a given vehicle speed U and a propulsion ratio, η, and they are given by

$$F_{Lift} = -\ Cm\ Q\ exp(|\alpha_E|) U_2 \sin \alpha_E \quad (11)$$

$$Fx = -\ Cm\ Q\ exp(|\alpha_E|) \cos \alpha_E\ (U - U_2 \cos \alpha_E) \quad (12)$$

$$U_2 = \frac{\frac{T}{M_E} + U\cos^2 \alpha_E}{\sin^2 \alpha_E + \cos^3 \alpha_E} \quad (13)$$

$$T = a\ (\eta\ U)^{\ b} = vehicle\ drag \quad (14)$$

where a and b are constants for the relationship between vehicle drag and speeds. The propulsion ratio, η, is defined as the ratio of commanded axial speed Uc to the actual axial speed U. At self-propulsion point the value of η is 1. The TVPJ thrust T is equal to the drag of the vehicle at self-propulsion point and can be written as a power function of U, given in equation (14).

The non-dimensional mass flow rate, Cm is an important factor that determines the stability contribution of the TVPJ[14]. The value for Cm can be determined from correlating against the model test data. For a given value of Cm at vehicle speed of U, the TVPJ-induced normal force and pitch moment on the vehicle over a range of angle of attack and propulsion ratio can be estimated from the above semi-empirical equations from (6) to (14). The propeller slipstream U_2 that is used to calculate the lift force of the inner control fin can also be found. The results in Fig. 2 show that the TVPJ induced normal force is about 40% of that on the vehicle body for speed of 6 knots.

IV. VALIDATION OF HYDRODYNAMIC MODEL

A. Tow Tank Test Description

A program of straight-line captive-LMRS UUV planar motion mechanism (PMM) test was performed in David Taylor Model Basin at Naval Surface Warfare Center (NSWC), Carderock Division, to determine the stability and control characteristics of the baseline vehicle. The test plan contains three separate plans (1) resistance and propulsion tests to determine the vehicle drag and TVPJ RPM at self-propulsion point, (2) stability and control tests to determine angle of attack statics and control fin effectiveness, and (3) over- and under-propulsion tests to determine the propulsion η effect on the control fins. Stripping tests were also conducted to isolate the effects of the recovery ring and its support struts. Fig.6 shows the full-scale test vehicle.

The PMM tests were conducted for the full-scale model at speeds from 3 to 6 knots to determine the hydrodynamic coefficients for the test vehicle by measuring the loads acting on the vehicle. The range of angle of attack was -18° to 18°, and the fin deflection angles were from -25° to 25°. The propulsion ratio range was 0.5 to 2.5. The testing produced significant amount of data presented in the final test report [15], which were used to validate the hydrodynamic model presented.

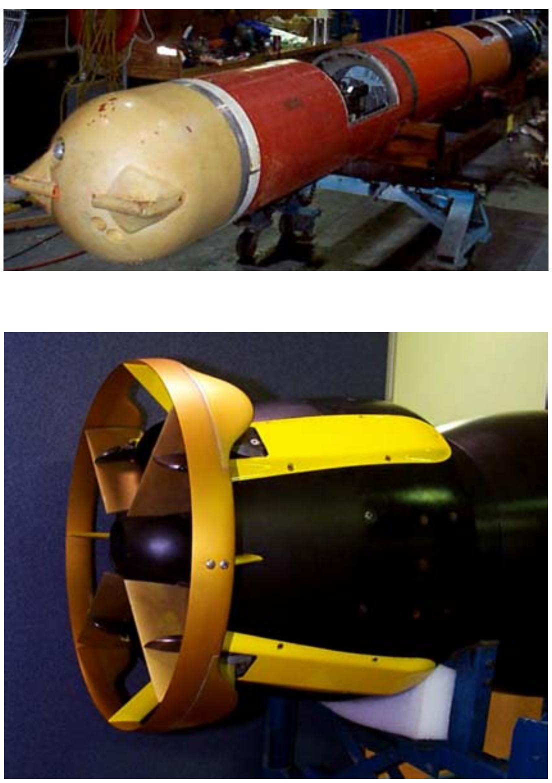

Fig. 6 Test vehicle, TVPJ, and after body

B. Prediction Verification for Baseline LMRS UUV

Under the body build-up method the hydrodynamic forces and moments on the vehicle were predicted as a function of angle of attack (AoA), velocity, propulsion ratio η, and control fin deflection. The results of prediction and measured data are shown in Fig. 2 and Fig. 7 to Fig. 14. Non-dimensional force and moment defined in 2510EOM [16] are used in all figures. The test data are shown as open or solid symbols and the predicted results are shown as solid or dashed lines.

The angle of attack (AoA) comparisons are presented in Fig. 2 for the 6-knot data and Fig. 7 for 3-knot data. The tare values of test data were shifted to match the predicted results at AoA=0°. The results are in good agreement for a range of AoA up to at least 12 degrees. It was noticed that the values of the measured data were different between positive AoA and negative AoA. For the positive region, the comparisons are in excellent agreement. Fig. 8 presents relative drag comparison in wind axis. The relative drag is defined as drag difference between some AoA and AoA=0°. The drag model shows very good agreement with the test data. The measured and predicted data for control fin effectiveness are shown in Fig.9 for self-propulsion condition. Good agreement are seen for sternplane angles of ±25° and angle of attack of ±6°. The axial force is also predicted well for deflected sternplane up to ±20°, as shown in Fig. 10 for 0° angle of attack and with shifted tare for test data at zero degree deflection.

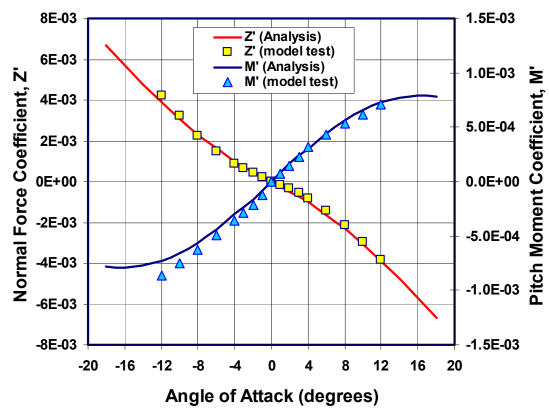

Fig. 7 Force and moment comparison, 3 knots

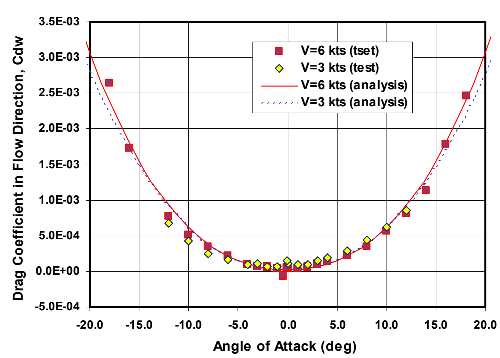

Fig. 8 Relative drag comparison

The correlation for the ring lift is shown in Fig. 11 for velocity range from 3 to 6 knots. The agreement between test data and predicted results is excellent for AoA values of ±4°. As angle of attack increases the discrepancies become larger. This indicates that the ring lift can not be described adequately by a linear model given in equation (5). Fig.12 and Fig.13 show the comparisons for η effect under various sternplane deflection conditions for the vehicle at zero angle of attack and speeds of 3 and 6 knots, respectively. At self-propulsion point (η =1) the agreement is excellent. For η greater than 1 and η less than 1, the TVPJ propulsor model over predicts lift for 6 knot speed condition. This discrepancy may be caused by over predicting the velocity of slipstream during acceleration and deceleration at speed of 6 knots. Under deceleration condition, both test and predicted data show that the control fins are less effective. Fig. 14 shows the comparisons of vehicle stability index, *Gv*, in vertical plane. Both the test data and predicted results show that the vehicle becomes less stable with increasing speed. The value of the stability index *Gv* is calculated using the following equation [15]:

$$G_v = 1 - \frac{M'_w (Z'_q + m')}{Z'_w (M'_q - x'_G m')} \qquad (15)$$

where m' is non-dimensional mass of vehicle and x'_G is the x coordinate of vehicle CG.

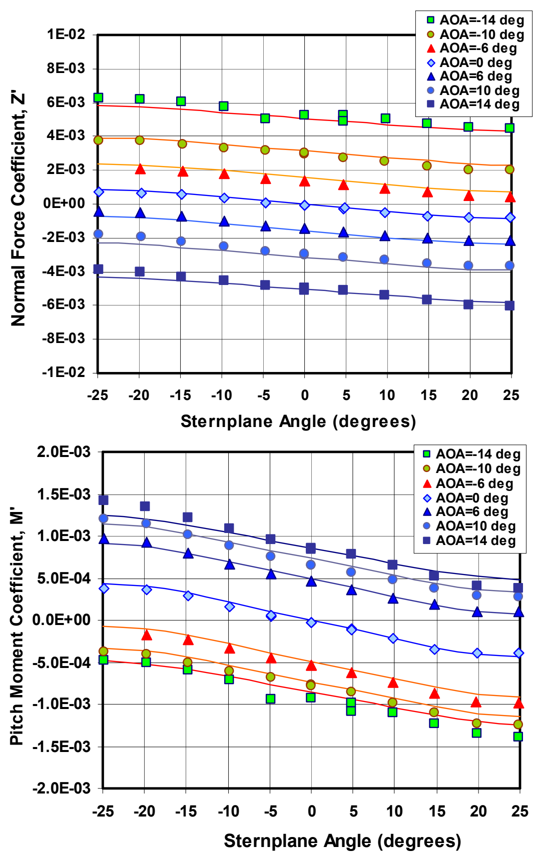

Fig. 9 Control fin derivative comparison, 6 knots

All the above comparisons with AoA data, control effectiveness, propulsor η effects, and *Gv* values at all speeds were carried out with the change in value of TVPJ mass flow rate, *Cm*. The changes in *Cm* value needed to correlate test and predicted data for all speeds are presented in Fig. 15. The results indicate that the non-dimensional mass flow rate decreases with increasing speed (or RPM). At lower speeds the *Cm* asymptotically approaches to 0.4, and at higher speeds the *Cm* decreases rapidly.

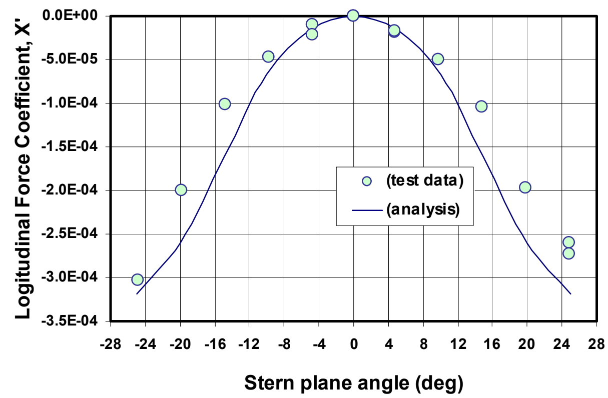

Fig. 10 Longitudinal force comparison, 6 knots

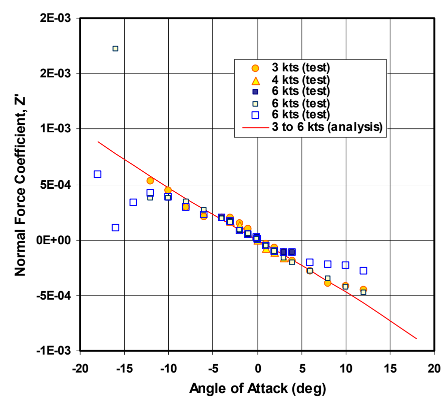

Fig. 11 Recovery ring model versus force, 6 knots

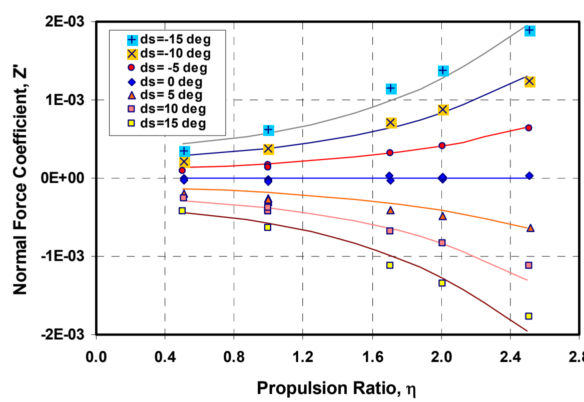

Fig. 12 TVPJ model versus force data, 3 knots

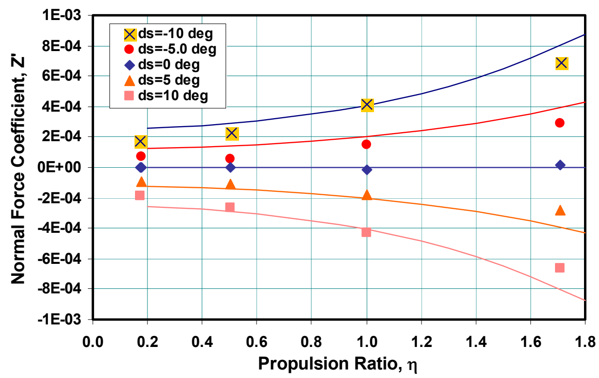

Fig. 13 TVPJ model versus force data, 6 knots

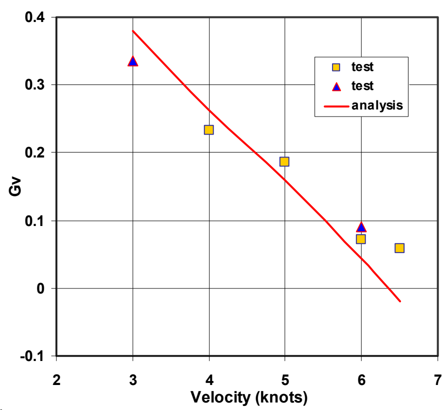

Fig. 14 Vehicle stability index, Gv, in vertical plane

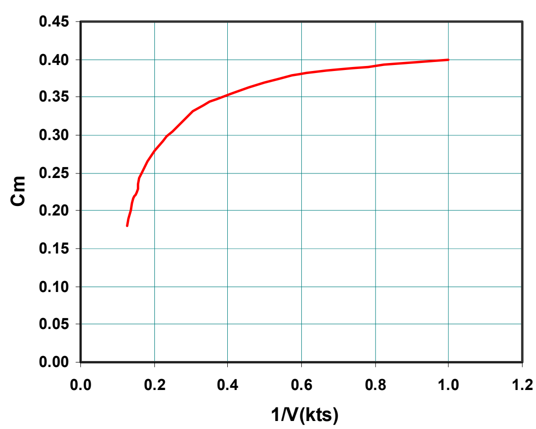

Fig. 15 Value of *Cm* versus vehicle speed

V. CONCLUSIONS

The application of body built-up method using semi-empirical hydrodynamic model was presented to predict the forces and moments for the LMRS UUV. The presented hydrodynamic model captures important hydrodynamic characteristics of the LMRS UUV, and the predicted results show very good agreements with tow tank test data. The results indicated that the vehicle stability is speed dependent and the control fin effectiveness decreases under deceleration conditions. Comparative results presented suggest future work to improve the TVPJ model to include the moment and drag of itself, and to extend the linear ring model to include nonlinear effects and proper stall behavior.

Acknowledgments

The author would like to thank The Boeing Company and the U.S Navy for granting the permission to publish this paper.

References

[1] R. Finck, "USAF Stability and Control Data Compendium (DATCOM)," Air Force Flight Dynamics Laboratory, Wright Patterson Air Force Base, April 1976.

[2] J.E. Fidler and C.A. Smith, " Methods for Predicting Submersible Hydrodynamic Characteristics," Naval Coastal Systems Center, *NCSC TM-238-78*, July 1978.

[3] M. R. Mendenhall, Editor, *Tactical Missile Aerodynamics: Prediction Methodology,* Vol. 142, Progress in Astronautics and Aeronautics, 1992.

[4] M. Munk, "The Aerodynamic Forces on Airship Hulls," *NACA Report 184,* 1924.

[5] H Allen and E. Perkins, "A Study of Effects of Viscosity on Flow Over Slender Inclined Bodies of Revolution," *NACA Report 1048,* 1951

[6] L. Jorgensen, "Prediction of Static Aerodynamic Characteristics for Space-Shuttle-like and Other Bodies at Angles of Attack from 0° to 180°," *NACA Technical Note D-6996,* 1973.

[7] R. Grady, Editor, *Hydroballistics Design Handbook*, Volume I, *SEAHAC TR 79-1*, January 1979.

[8] R. Peterson, "Evaluation of Semi-Empirical Methods for Predicting Linear Static and Rotary Hydrodynamic Coefficients," *NCSC TM-291-80*, June 1980.

[9] S. Hoerner, *Fluid-Dynamic Lift*. Hoerner Fluid Dynamics, 1985.

[10] E. Lewis, Editor, *Principles of Naval Architecture,* Second Revision, Vol. III, 1989.

[11] W. Pitts, J. Nielsen, and G. Kaattari, "Lift and Center of Pressure of Wing-Body-Tail Combinations at Subsonic, Transonic, and Supersonic Speeds," *NACA Report. 1307*, 1957.

[12] J.N. Nielsen, *Missile Aerodynamics, McGraw-Hill, New York,* 1960.

[13] B.W. McCormick, "Effect of a Centerbody on a Ring-Wing," PennState Applied Research Laboratory Technical Memo. No.5.2420-05, 1959.

[14] D.E. Humphreys and N.S. Smith, "Hydrodynamic & Control Model for the (AN/BLQ-11 UUV) LMRS Vehicle," *VCT Report No. 60*, February 2001.

[15] R.F. Roddy, "Quick Look Report of the Stability and Control Characteristics of the LMRS UUV in Open Water and behind the Recovery Arm," *NSWC Report*, July 2000.

[16] M. Gertler and G.R. Hagen, "Standard Equations of Motion for Submarine Simulations," *DTNSRDC Report 2510*, June 1967.